

First multidimensional, high precision measurements of semi-inclusive π^+ beam single spin asymmetries from the proton over a wide range of kinematics

S. Diehl,^{34,6} A. Kim,⁶ G. Angelini,¹³ K. Joo,⁶ S. Adhikari,¹¹ M. Amaryan,³³ M. Arratia,⁵ H. Atac,⁴³ H. Avakian,⁴⁴ C. Ayerbe Gayoso,⁵¹ N.A. Baltzell,⁴⁴ L. Barion,¹⁵ S. Bastami,⁶ M. Battaglieri,^{44,17} I. Bedlinskiy,²⁸ F. Benmokhtar,⁸ A. Bianconi,^{47,20} A.S. Biselli,⁹ M. Bondi,¹⁷ F. Bossù,³ S. Boiarinov,⁴⁴ K.-T. Brinkmann,³⁴ W.J. Briscoe,¹³ W. Brooks,⁴⁵ D. Bulumulla,³³ V.D. Burkert,⁴⁴ D.S. Carman,⁴⁴ J.C. Carvajal,¹¹ A. Celentano,¹⁷ P. Chatagnon,²¹ T. Chetry,^{27,32} G. Ciullo,^{15,10} L. Clark,⁴⁸ B.A. Clary,⁶ P.L. Cole,²⁵ M. Contalbrigo,¹⁵ G. Costantini,^{47,20} V. Crede,¹² A. D'Angelo,^{18,37} N. Dashyan,⁵² R. De Vita,¹⁷ M. Defurne,³ A. Deur,⁴⁴ C. Dilks,⁷ C. Djalali,³² M. Dugger,² R. Dupre,²¹ M. Ehrhart,^{1,21} A. El Alaoui,⁴⁵ L. El Fassi,²⁷ L. Elouadrhiri,⁴⁴ S. Fegan,⁴⁹ A. Filippi,¹⁹ T. Forest,¹⁴ G. Gavalian,⁴⁴ G.P. Gilfoyle,³⁶ F.X. Girod,⁴⁴ D.I. Glazier,⁴⁸ A.A. Golubenko,⁴¹ R.W. Gothe,⁴² Y. Gotra,⁴⁴ K.A. Griffioen,⁵¹ M. Guidal,²¹ K. Hafidi,¹ H. Hakobyan,^{45,52} M. Hattawy,³³ T.B. Hayward,⁵¹ D. Heddle,^{4,44} K. Hicks,³² A. Hobart,²¹ M. Holtrop,²⁹ C.E. Hyde,³³ D.G. Ireland,⁴⁸ E.L. Isupov,⁴¹ H.S. Jo,²⁴ R. Johnston,²⁶ S. Joosten,¹ D. Keller,⁵⁰ M. Khachatryan,³³ A. Khanal,¹¹ W. Kim,²⁴ A. Kripko,³⁴ V. Kubarovsky,⁴⁴ S.E. Kuhn,³³ L. Lanza,¹⁸ M. Leali,^{47,20} S. Lee,²⁶ P. Lenisa,^{15,10} K. Livingston,⁴⁸ Z. Lu,³⁸ I.J.D. MacGregor,⁴⁸ D. Marchand,²¹ N. Markov,^{44,6} L. Marsicano,¹⁷ V. Mascagna,^{46,20} B. McKinnon,⁴⁸ Z.E. Meziani,^{1,43} R.G. Milner,²⁶ T. Mineeva,⁴⁵ M. Mirazita,¹⁶ V. Mokeev,⁴⁴ P. Moran,²⁶ A. Movsisyan,¹⁵ C. Munoz Camacho,²¹ P. Nadel-Turonski,⁴⁴ P. Naidoo,⁴⁸ K. Neupane,⁴² S. Niccolai,²¹ G. Niculescu,²³ T.R. O'Connell,⁶ M. Osipenko,¹⁷ M. Paolone,^{30,43} L.L. Pappalardo,^{15,10} R. Paremuzyan,^{44,29} E. Pasyuk,⁴⁴ W. Phelps,⁴ O. Pogorelko,²⁸ Y. Prok,³³ A. Prokudin,⁶ B.A. Raue,^{11,44} M. Ripani,¹⁷ J. Ritman,²² A. Rizzo,^{18,37} C.D. Roberts,³⁹ P. Rossi,^{44,16} J. Rowley,³² F. Sabatié,³ C. Salgado,³¹ A. Schmidt,¹³ E.P. Segarra,²⁶ Y.G. Sharabian,⁴⁴ U. Shrestha,³² O. Soto,^{16,45} N. Sparveris,⁴³ S. Stepanyan,⁴⁴ P. Stoler,³⁵ I.I. Strakovsky,¹³ S. Strauch,⁴² K. Tezgin,⁶ A. Thornton,⁴⁸ N. Tyler,⁴² R. Tyson,⁴⁸ M. Ungaro,⁴⁴ L. Venturelli,^{47,20} H. Voskanyan,⁵² A. Vossen,⁷ E. Voutier,²¹ D.P. Watts,⁴⁹ K. Wei,⁶ X. Wei,⁴⁴ S.-S. Xu,⁴⁰ B. Yale,⁵¹ N. Zachariou,⁴⁹ and J. Zhang⁵⁰

(The CLAS Collaboration)

¹Argonne National Laboratory, Argonne, Illinois 60439

²Arizona State University, Tempe, AZ 85281

³IRFU, CEA, Université Paris-Saclay, F-91191 Gif-sur-Yvette, France

⁴Christopher Newport University, Newport News, Virginia 23606

⁵University of California, Riverside, CA 92521

⁶University of Connecticut, Storrs, Connecticut 06269

⁷Duke University, Durham, North Carolina 27708-0305

⁸Duquesne University, 600 Forbes Avenue, Pittsburgh, PA 15282

⁹Fairfield University, Fairfield CT 06824

¹⁰Università di Ferrara, 44121 Ferrara, Italy

¹¹Florida International University, Miami, Florida 33199

¹²Florida State University, Tallahassee, Florida 32306

¹³The George Washington University, Washington, DC 20052

¹⁴Idaho State University, Pocatello, ID 83209

¹⁵INFN, Sezione di Ferrara, 44100 Ferrara, Italy

¹⁶INFN, Laboratori Nazionali di Frascati, 00044 Frascati, Italy

¹⁷INFN, Sezione di Genova, 16146 Genova, Italy

¹⁸INFN, Sezione di Roma Tor Vergata, 00133 Rome, Italy

¹⁹INFN, Sezione di Torino, 10125 Torino, Italy

²⁰INFN, Sezione di Pavia, 27100 Pavia, Italy

²¹Université Paris-Saclay, CNRS/IN2P3, IJCLab, 91405 Orsay, France

²²Institute für Kernphysik (Juelich), Juelich, Germany

²³James Madison University, Harrisonburg, Virginia 22807

²⁴Kyungpook National University, Daegu 41566, Republic of Korea

²⁵Lamar University, 4400 MLK Blvd, PO Box 10046, Beaumont, Texas 77710

²⁶Massachusetts Institute of Technology, Cambridge, Massachusetts 02139-4307

²⁷Mississippi State University, Mississippi State, MS 39762-5167

²⁸National Research Centre Kurchatov Institute - ITEP, Moscow, 117259, Russia

²⁹University of New Hampshire, Durham, New Hampshire 03824-3568

³⁰New Mexico State University, PO Box 30001, Las Cruces, NM 88003, USA

³¹Norfolk State University, Norfolk, Virginia 23504

³²Ohio University, Athens, Ohio 45701

- ³³Old Dominion University, Norfolk, Virginia 23529
³⁴II. Physikalisches Institut der Universität Gießen, 35392 Gießen, Germany
³⁵Rensselaer Polytechnic Institute, Troy, New York 12180-3590
³⁶University of Richmond, Richmond, Virginia 23173
³⁷Università di Roma Tor Vergata, 00133 Rome Italy
³⁸School of Physics, Southeast University, Nanjing 211189, Jiangsu, China
³⁹School of Physics and Institute for Nonperturbative Physics, Nanjing University, Nanjing 210093, Jiangsu, China
⁴⁰School of Science, Nanjing University of Posts and Telecommunications, Nanjing 210023, Jiangsu, China
⁴¹Skobeltsyn Institute of Nuclear Physics, Lomonosov Moscow State University, 119234 Moscow, Russia
⁴²University of South Carolina, Columbia, South Carolina 29208
⁴³Temple University, Philadelphia, PA 19122
⁴⁴Thomas Jefferson National Accelerator Facility, Newport News, Virginia 23606
⁴⁵Universidad Técnica Federico Santa María, Casilla 110-V Valparaíso, Chile
⁴⁶Università degli Studi dell'Insubria, 22100 Como, Italy
⁴⁷Università degli Studi di Brescia, 25123 Brescia, Italy
⁴⁸University of Glasgow, Glasgow G12 8QQ, United Kingdom
⁴⁹University of York, York YO10 5DD, United Kingdom
⁵⁰University of Virginia, Charlottesville, Virginia 22901
⁵¹College of William and Mary, Williamsburg, Virginia 23187-8795
⁵²Yerevan Physics Institute, 375036 Yerevan, Armenia

High precision measurements of the polarized electron beam-spin asymmetry in semi-inclusive deep inelastic scattering (SIDIS) from the proton have been performed using a 10.6 GeV incident electron beam and the CLAS12 spectrometer at Jefferson Lab. We report here the first multidimensional study of single π^+ SIDIS data over a large kinematic range in z , x_B , P_T and virtualities Q^2 ranging from 1 GeV² up to 7 GeV². In particular, the structure function ratio $F_{LU}^{\sin\phi}/F_{UU}$ has been determined, where $F_{LU}^{\sin\phi}$ is a twist-3 quantity that can reveal novel properties of quark-gluon correlations within the nucleon. The impact of the data on the evolving understanding of the underlying reaction mechanisms and their kinematic variation is explored using theoretical models for the different contributing transverse momentum dependent parton distribution functions.

PACS numbers: 75.25.-j, 13.60.-r, 13.88.+e, 24.85.+p

Many decades of experiments in deep inelastic scattering (DIS) of lepton beams off nucleons have mapped out the momentum distributions in the nucleon in terms of one-dimensional (1-D) parton distribution functions (PDFs) [1–3]. While these measurements provided significant insight into the structure of the nucleon, many important and interesting aspects of the nucleon structure cannot be revealed in this 1-D picture since PDFs are essentially averaged over all degrees of freedom except the longitudinal momentum. Therefore, they cannot address questions such as: Do quarks undergo orbital motion? Is there a connection between the motion of quarks, their spin and the spin of the proton? How is the total spin of the proton built up from the spin and the orbital angular momentum of partons? Today, the possibility of three-dimensional (3-D) imaging exists, which allows such questions to be addressed [4–9]. Remarkable theoretical advances over the past decade have led to a rigorous framework where information on the confined motion of the partons inside a fast moving nucleon is matched to transverse momentum dependent parton distribution functions (TMDs) [6–8, 10]. In particular, TMDs can encode information about the orbital motion of quarks in the parent nucleon and correlations between the motion of partons and their spin.

Semi-inclusive DIS (SIDIS), where a specified hadron

is detected in the final state, is a powerful tool to study the transverse structure of the nucleon. Spin asymmetries in polarized SIDIS are directly related to TMDs and fragmentation functions (FFs), and are the subject of intense theoretical and experimental studies [11–16]. Recently, sizable non-vanishing single spin asymmetries (SSAs) have been observed in SIDIS with longitudinally polarized electron beams and unpolarized targets (in the following referred to as beam SSAs) [17–21]. Since beam SSAs are subleading twist-3 objects, they are expected to be suppressed by $\mathcal{O}(M/Q)$, where M is the target mass and Q^2 is the photon virtuality. However, with the energies available at existing fixed-target facilities, contributions of the order $\mathcal{O}(M/Q)$ could be sizable, making such twist-3 contributions accessible and thereby providing access to the information they contain about quark-gluon correlations.

In this Letter, for the first time, we present beam SSAs and extract the $\sin\phi$ moment $A_{LU}^{\sin\phi}$ in π^+ SIDIS of longitudinally polarized electrons off unpolarized protons with a wide range of fully differential multidimensional kinematics in the Q^2 range from 1.7 to 7.0 GeV², x_B from 0.13 - 0.52, z from 0.18 - 0.7 and P_T up to 0.85 GeV ($c = 1$). Here we define the fraction of the proton's momentum carried by the struck quark as x_B , the energy fraction of the incoming lepton carried by the virtual photon as y ,

the energy fraction of the virtual photon carried by the outgoing hadron as z , the transverse momentum of the final state hadron as P_T and the virtuality of the collision as Q^2 . The diagram in Fig. 1(a) shows the SIDIS scattering process, including the involved TMDs and FFs, and Fig. 1(b) shows the definition of the reaction kinematics.

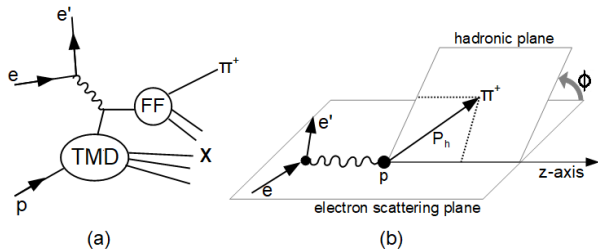


FIG. 1: (a) Schematic diagram of the single pion semi-inclusive deep inelastic scattering process with the involved parton distributions and fragmentation functions. (b) Definition of the reaction kinematics of single pion SIDIS.

In the one-photon exchange approximation beam SSAs are defined as follows:

$$SSA(z, P_T, \phi, x_B, Q^2) = \frac{d\sigma^+ - d\sigma^-}{d\sigma^+ + d\sigma^-} \quad (1)$$

$$= \frac{A_{LU}^{\sin\phi} \sin\phi}{1 + A_{UU}^{\cos\phi} \cos\phi + A_{UU}^{\cos 2\phi} \cos 2\phi},$$

where $d\sigma^\pm$ is the differential cross section for each beam helicity state (\pm). For the positive / negative helicity the spin is parallel / anti-parallel to the beam direction. The subscripts of the moments A_{ij} represent the longitudinally polarized (L) or unpolarized (U) state of the beam and the target, respectively. ϕ is the azimuthal angle between the electron scattering plane and the hadronic reaction plane (see Fig. 1 (b)).

The $\sin\phi$ moment $A_{LU}^{\sin\phi}$ is proportional to the polarized structure function $F_{LU}^{\sin\phi}$:

$$A_{LU}^{\sin\phi} = \frac{\sqrt{2\epsilon(1-\epsilon)} F_{LU}^{\sin\phi}}{F_{UU,T} + \epsilon F_{UU,L}}, \quad (2)$$

where the structure functions in $F_{UU} = F_{UU,T} + \epsilon F_{UU,L}$ correspond to the longitudinal and transverse polarizations of the virtual photon, and ϵ is the ratio of their fluxes.

This study focuses on the $A_{LU}^{\sin\phi}$ asymmetry and thus on the structure function $F_{LU}^{\sin\phi}$, which is related to the quark-gluon-quark correlations in the proton (twist-3). Assuming factorization, it can be expressed as a convo-

lution, denoted by \mathcal{C} , of TMDs and FFs [8, 22]:

$$F_{LU}^{\sin\phi} = \frac{2M}{Q} \mathcal{C} \left[-\frac{\hat{h} \cdot k_T}{M_h} \left(x_B e H_1^\perp + \frac{M_h}{M} f_1 \frac{\tilde{G}^\perp}{z} \right) + \frac{\hat{h} \cdot P_T}{M} \left(x_B g^\perp D_1 + \frac{M_h}{M} h_1^\perp \frac{\tilde{E}}{z} \right) \right]. \quad (3)$$

Here e is a twist-3 PDF, H_1^\perp is the Collins FF, f_1 is an unpolarized distribution function, \tilde{G}^\perp is a twist-3 FF, g^\perp is a twist-3 T-odd distribution function, D_1 is an unpolarized FF, h_1^\perp is the Boer-Mulders function and \tilde{E} is a twist-3 FF. k_T is the transverse quark momentum, M_h is the pion mass and \hat{h} is a unit vector in the direction of the pion. Every term in the structure function $F_{LU}^{\sin\phi}$ is a so-called genuine twist-3 term, *e.g.* related to quark-gluon correlators (or current quark mass terms) [8]. Hence, the often used Wandzura-Wilczek approximation, which neglects all interaction-dependent parts in the twist-3 terms in a structure function, is not valid in this case as it would demand the entire asymmetry to be zero [23], which is not the case.

Since the magnitude of the observed asymmetry of several percent cannot be explained by perturbative QCD, several mechanisms have been proposed to generate such an asymmetry. One mechanism involves the eH_1^\perp term [24, 25], which indicates that the asymmetry results from the coupling of the distribution function $e(x)$ with the Collins FF H_1^\perp . Other mechanisms relate to the convolution of the Boer-Mulders function h_1^\perp with the FF \tilde{E} and to the coupling between the unpolarized distribution function f_1 and the twist-3 FF \tilde{G}^\perp . Apart from the ones mentioned above, a mechanism involving the poorly known twist-3 TMD distribution function g^\perp can also give rise to the beam SSA. g^\perp appears in the decomposition of the quark correlator if the dependence on the light-cone vector is included. In order to model the twist-3 T-odd chiral-even TMD g^\perp it is necessary to take into account final state interactions, which can be taken into account by one-gluon exchange. Therefore, studying beam SSAs provides a unique opportunity to unravel the role of genuine twist-3 quark-gluon correlation effects.

SIDIS π^+ electroproduction was measured at Jefferson Lab with CLAS12 (CEBAF Large Acceptance Spectrometer for experiments at 12 GeV) [26]. Beam single spin asymmetries were extracted over a wide range in Q^2 , x_B , z , P_T and ϕ . The incident electron beam was longitudinally polarized and had an energy of 10.6 GeV. The target was unpolarized liquid hydrogen. The CLAS12 forward detector consists of six identical sectors within a toroidal magnetic field. The momentum and the charge of the particles were determined by 3 regions of drift chambers from the curvature of the particle trajectories in the magnetic field. The electron identification was based on a lead-scintillator electromagnetic sampling calorimeter in combination with a Cherenkov counter.

Positive pions were identified by time-of-flight measurements. For the selection of deeply inelastic scattered electrons, cuts on $Q^2 > 1 \text{ GeV}^2$, $y < 0.75$ and on the invariant mass of the hadronic final state $W > 2 \text{ GeV}$, were applied. In addition, it was required that the $e'\pi^+X$ missing mass be larger than 1.5 GeV to minimize the contribution from exclusive channels.

Figure 2 shows the new CLAS12 data as a function of x_B , z and P_T integrated over all other kinematic variables in comparison to the available world data for $F_{LU}^{\sin\phi}/F_{UU}$ from previous experiments. Details on the multidimensional analysis for CLAS12 follow. Even though $F_{LU}^{\sin\phi}$

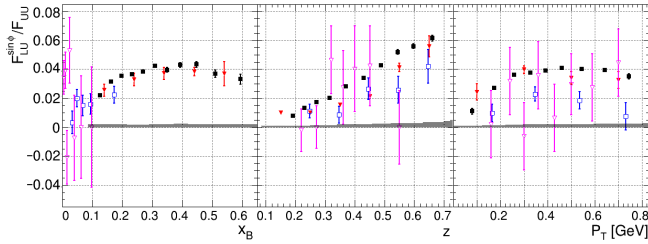


FIG. 2: CLAS12 data (filled squares), compared with the available world data from HERMES [19] (open squares), COMPASS [20] (open triangles) and CLAS [21] (filled triangles) for $F_{LU}^{\sin\phi}/F_{UU}$ as a function of x_B , z and P_T integrated over all other kinematic variables. It has to be noted that the different experiments apply slightly different cuts on the kinematic variables and that in the case of COMPASS all positive hadrons are considered. The $A_{LU}^{\sin\phi}$ values stated in the References were transformed to $F_{LU}^{\sin\phi}/F_{UU}$ following Eq. (2). The grey histogram shows the systematic uncertainty of the present data.

has been studied at HERMES [18, 19], COMPASS [20] and CLAS [21] during the last two decades, there is still no consistent understanding of the contribution of each part to the total structure function. One of the main reasons for this can be seen in the low statistics and the resulting large uncertainties or limited kinematic coverage of many previous experiments. The high statistics on an extended kinematic range, which is available with the new CLAS12 data, enables a fully differential multidimensional analysis for the first time and therefore provides an excellent basis for the extraction of TMDs and FFs.

For the multidimensional binning, first the electron variables are sorted in 9 bins in Q^2 and x_B (see Fig. 3). For each of these $Q^2 - x_B$ bins a binning is applied to z and P_T as shown for the example of $Q^2 - x_B$ bin 1 in Fig. 3.

The beam SSA and its statistical uncertainty were determined experimentally from the number of counts with positive and negative helicity (N_i^\pm) in a specific bin i as:

$$SSA = \frac{1}{P_e} \frac{N_i^+ - N_i^-}{N_i^+ + N_i^-}, \quad \sigma_{SSA} = \frac{1}{P_e} \sqrt{\frac{1 - (P_e SSA)^2}{N_i^+ + N_i^-}}, \quad (4)$$

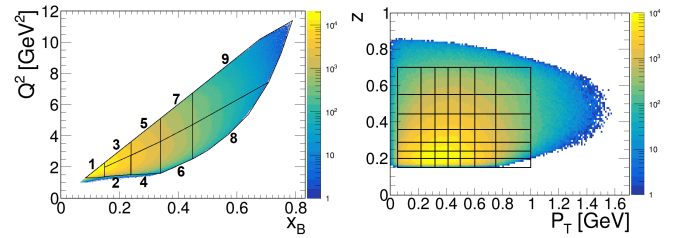


FIG. 3: Left: Correlation between Q^2 and x_B . The bin borders are shown as black lines and the bin numbering is given. Right: Correlation between z and P_T for $Q^2 - x_B$ - bin 1. The black lines indicate the bin borders.

where P_e is the average magnitude of the beam polarization. P_e was measured with a Møller polarimeter upstream of CLAS12 and was $86.3\% \pm 2.6\%$.

To extract the $\sin\phi$ moment, $A_{LU}^{\sin\phi}$, the beam SSA was measured as a function of the azimuthal angle ϕ . Then the data was fit with a $\sin\phi$ function. Figure 4 shows the beam SSA as a function of ϕ for two typical multidimensional bins. As expected the ϕ -dependence

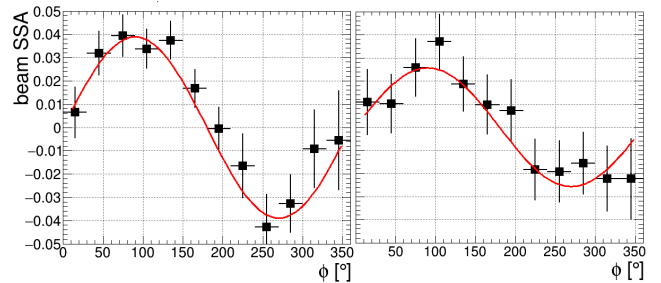


FIG. 4: Beam SSA as a function of ϕ for two typical bins (left: $Q^2 = 1.98 \text{ GeV}^2$, $x_B = 0.20$, $P_T = 0.25 \text{ GeV}$, $z = 0.65$; right: $Q^2 = 6.5 \text{ GeV}^2$, $x_B = 0.53$, $P_T = 0.29 \text{ GeV}$, $z = 0.44$). The vertical bars show the statistical uncertainty of each point, while the horizontal bars correspond to the bin width. The red line shows the fit with a $\sin\phi$ function.

can be well described by a $\sin\phi$ function. The obtained $A_{LU}^{\sin\phi}$ moment is then related to $F_{LU}^{\sin\phi}/F_{UU}$ via Eq. (2).

Several sources of systematic uncertainty were investigated, including beam polarization, radiative effects, particle identification and contamination from baryon resonances and exclusive ρ meson production. A detailed Monte Carlo simulation was performed to study acceptance and bin-migration effects, which were both found to be negligible compared to the other contributions. The influence of additional azimuthal modulations $\cos\phi$ and $\cos 2\phi$ on the extracted $\sin\phi$ amplitude was also evaluated, and found to be negligible. The total systematic uncertainty in each bin is defined as the square-root of the quadratic sum of the uncertainties from all sources. It is typically on the order of 6.4% and dominated by the uncertainty from radiative effects (3.0%) and from the

beam polarization (3.0%).

The structure function ratio $F_{LU}^{\sin\phi}/F_{UU}$ has been extracted for each of the obtained 344 bins. The result for each bin, as well as the mean value of the kinematic variables in each bin, are provided in the supplemental material and in the CLAS physics database [27, 28]. Figure 5 (6) shows the z (P_T) dependence for selected P_T (z) bins in different bins of Q^2 and x_B , which represent the characteristics of the different kinematic regions. The results are compared to theoretical predictions, which have been calculated based on the models presented in Refs. [29] and [30] (models 1 and 2) and Ref. [31] (model 3).

The first two models describe the proton as an active quark plus (inert) spectator scalar and axial-vector diquarks. Both models include the eH_1^\perp and $g^\perp D_1$ terms of the structure function, while the other terms are assumed to be small. Model 1 uses a complicated propagator for the axial-vector diquark and the ratio of axial-vector-diquark/scalar-diquark strengths fitted [32] to ZEUS [33] and GRSV01 [34] distribution functions (DFs). Diquark masses and various cutoffs are also parameters included in the fit to the DFs. The fit produces $|I = 1, I_z = 1\rangle$ and $|I = 1, I_z = 0\rangle$ axial-vector diquarks with very different masses. Notably, this outcome conflicts with direct calculations of diquark masses, in which these correlations are typically degenerate [35]. Model 2 uses a simple propagator for axial-vector diquarks and the ratio of axial-vector-diquarks and scalar-diquarks is fixed by SU(4) spin-flavour symmetry. The model also uses mass degenerate axial-vector diquarks. The models differ most significantly in the form of the propagator for the axial-vector diquark (complex versus simple) and the masses of these correlations (different versus degenerate). The FFs used in both models are described in Ref. [36].

Model 3 includes only the eH_1^\perp term with the Collins function taken from the parameterization of Ref. [15] and $e(x)$ based on the chiral quark soliton model [25, 37, 38]. This is the only model predicting the experimentally not measurable $\delta(x)$ -contribution in $e(x)$ expected in QCD and related to the pion-nucleon sigma term [24].

For the experimental data it can be observed that the z dependence changes from a more flat behaviour at small P_T , Q^2 , and x_B values to a steep increase at large P_T , Q^2 , and x_B values. Also for the P_T dependence a small magnitude with a nearly flat behaviour can be observed at small Q^2 , x_B , and z values, while for increasing z values a peaking structure with varying mean value and width can be observed at small Q^2 and x_B , while an increasing trend becomes dominant at large Q^2 and x_B values.

The best reproduction of the general trend is provided by model 2. For this model, the comparison of the different kinematic regions shows, that while eH_1^\perp is the dominant term at small Q^2 and x_B values, $g^\perp D_1$ becomes more and more important for the description of the behaviour at large Q^2 and x_B . Model 1 mixes a

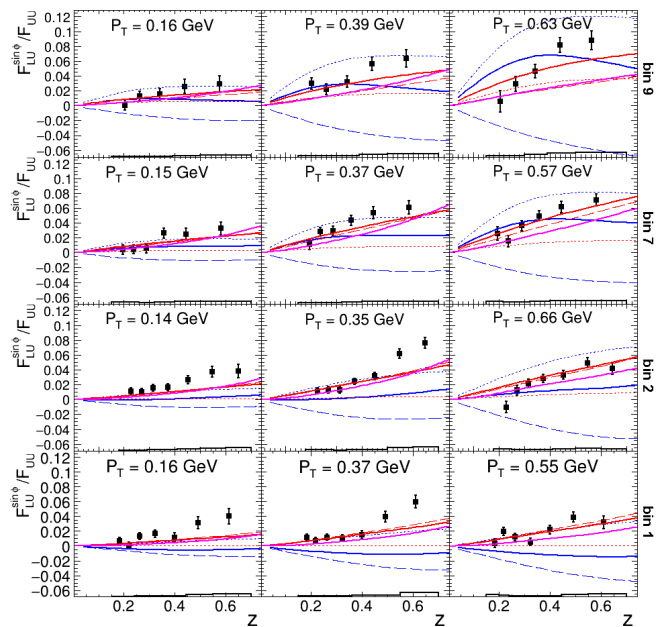


FIG. 5: z dependence of $F_{LU}^{\sin\phi}/F_{UU}$ for increasing P_T (left to right) and for different Q^2 - x_B bins (bin 1: $Q^2 = 1.71$ GeV 2 , $x_B = 0.13$, bin 2: $Q^2 = 2.02$ GeV 2 , $x_B = 0.19$, bin 7: $Q^2 = 4.89$ GeV 2 , $x_B = 0.39$, bin 9: $Q^2 = 6.55$ GeV 2 , $x_B = 0.52$). The systematic uncertainty is given by the histogram just above the horizontal axis. The predictions of the different theoretical models are shown by the bold lines (blue: model 1, red: model 2, magenta: model 3). For models 1 and 2 the contribution from eH_1^\perp (dashed line) and $g^\perp D_1$ (dotted line) are shown in the same color as the final result.

complicated axial-vector diquark propagator with a simple proton wave function and uses vastly different masses for diquarks within the same isospin multiplet. Here it is seen to be challenged by high precision experiments. The simplicity and, hence, internal consistency of model 2 is more natural beginning for phenomenological explorations. Even though model 3 uses a different approach, it provides results that are very similar to the eH_1^\perp term of model 2, which provides an additional support for this model and, possibly, points to an important role for axial-vector diquarks in the proton's wave function.

Importantly, these theory-experiment comparisons highlight the discriminating power of a fully multidimensional analysis with high statistics over a wide kinematic range. Such data provides both the means of verifying the reliability of different models and their underlying assumptions, and the ability to place increasingly tight constraints on the TMDs involved.

Since a fully multidimensional analysis is herein made available for the first time, some issues with model 2 are also exposed, especially in the finer details. This indicates that either the parametrisation of the involved TMDs and FFs has to be improved or that additional terms from Eq. (3) besides the two that have been used

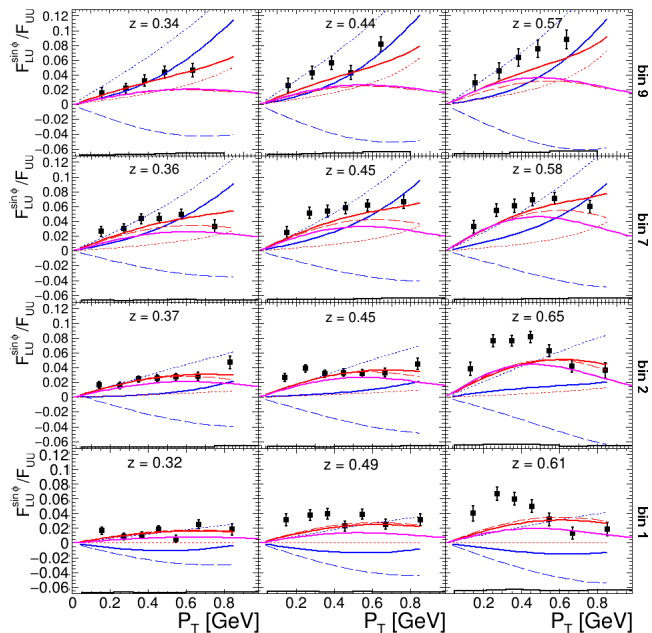


FIG. 6: P_T dependence of $F_{LU}^{\sin\phi}/F_{UU}$ for increasing z bins (left to right) and for different Q^2 - x_B bins (bin 1: $Q^2 = 1.71$ GeV 2 , $x_B = 0.13$, bin 2: $Q^2 = 2.02$ GeV 2 , $x_B = 0.19$, bin 7: $Q^2 = 4.89$ GeV 2 , $x_B = 0.39$, bin 9: $Q^2 = 6.55$ GeV 2 , $x_B = 0.52$). The systematic uncertainty is given by the histogram just above the horizontal axis. The predictions of the different theoretical models are shown by the bold lines (blue: model 1, red: model 2, magenta: model 3). For models 1 and 2 the contribution from eH_1^\perp (dashed line) and $g^\perp D_1$ (dotted line) are shown in the same color as the final result.

provide sizable contributions in some kinematic regions. Therefore, including the multidimensional data points presented in this work will help to further constrain the TMDs and FFs in global fits.

In addition to the z and P_T dependence, the x_B dependence can also provide valuable insights into the kinematic dependence of the involved TMDs and FFs. The result for the x_B dependence are shown in Fig. 7. To obtain these dependences, the same multidimensional binning is used. Owing to the correlation between x_B and Q^2 , the x_B dependence is integrated/averaged over Q^2 . Therefore, only discrete points are shown for the theory calculations. Also as a function of x_B a strong kinematic dependence of the behaviour can be observed, with a more flat behaviour at small z and P_T and an increasing trend for larger P_T and z values. As for the z and P_T dependence, the best agreement is provided by model 2. The x_B dependence clearly shows that model 3, which uses only the eH_1^\perp term, provides a sufficient description at small z and P_T , but cannot reproduce the trend at the largest P_T and z values.

The structure function ratio $F_{LU}^{\sin\phi}/F_{UU}$ corresponding to the polarized electron beam single spin asymmetry in semi-inclusive deep inelastic scattering has been

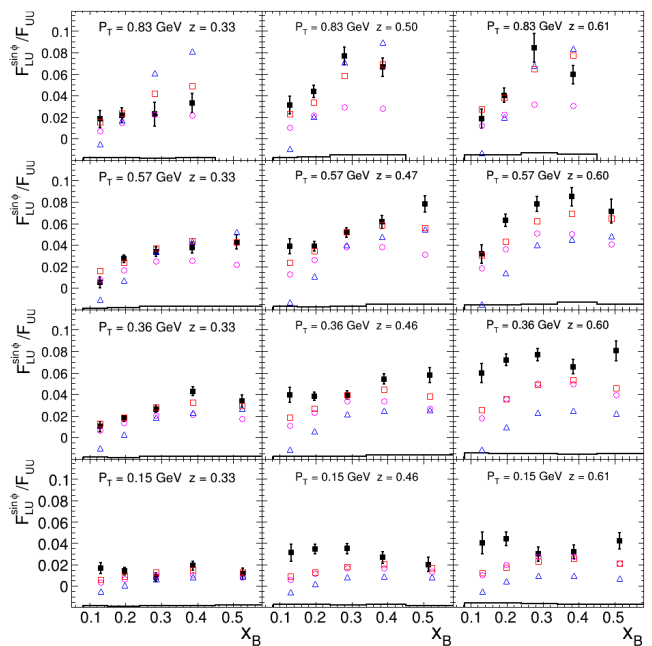


FIG. 7: x_B dependence of $F_{LU}^{\sin\phi}/F_{UU}$ for selected P_T and z bins. The result is integrated over Q^2 . The systematic uncertainty is given by the histogram just above the horizontal axis. The predictions of the different theoretical models are shown as open symbols (blue triangles: model 1, red squares: model 2, magenta circles: model 3).

measured over a wide range of kinematics in a fully multidimensional study for the first time. The comparison with calculations allows a clear differentiation between competing reaction models, *e.g.* highlighting the importance of the poorly known T-odd chiral-even TMD g^\perp at large P_T and z , while providing new empirical information in support of an important role for axial-vector diquark correlations in the proton's wave function. Therefore, including this multidimensional measurement into global fits, in combination with future measurements of unpolarized cross sections, as well as polarized target spin asymmetries, will provide new, strong constraints on the participating TMDs and FFs. Such progress will set us firmly on the path to a deeper understanding of nucleon structure in the 3-D space most natural to picturing composite objects in relativistic quantum field theory.

We acknowledge the outstanding efforts of the staff of the Accelerator and the Physics Divisions at Jefferson Lab in making this experiment possible. We owe much gratitude to P. Schweitzer for many fruitful discussions concerning the interpretation of our results. This work was supported in part by the U.S. Department of Energy, the National Science Foundation (NSF), the Italian Istituto Nazionale di Fisica Nucleare (INFN), the French Centre National de la Recherche Scientifique (CNRS), the French Commissariat pour l'Energie Atomique, the UK Science and Technology Facilities Coun-

cil, the National Research Foundation (NRF) of Korea, the Helmholtz-Forschungsakademie Hessen für FAIR (HFHF), the Ministry of Science and Higher Education of the Russian Federation and the National Natural Science Foundation of China. The Southeastern Universities Research Association (SURA) operates the Thomas Jefferson National Accelerator Facility for the U.S. Department of Energy under Contract No. DE-AC05-06OR23177.

-
- [1] J. Gao, L. Harland-Lang and J. Rojo, Phys. Rept. **742**, 1 (2018).
- [2] J. J. Ethier and E. R. Nocera, Annu. Rev. Nucl. Part. Sci. **70**, 43 (2020).
- [3] K.Kovarik, P.M. Nadolsky and D.E. Soper, Rev. Mod. Phys. **92**, 045003 (2020).
- [4] A. Kotzinian, Nucl. Phys. B **441**, 234 (1995).
- [5] P. J. Mulders and R. D. Tangerman, Nucl. Phys. B **461**, 197 (1996).
- [6] D. Boer and P. J. Mulders, Phys. Rev. D **57**, 5780 (1998).
- [7] K. Goeke, A. Metz and M. Schlegel, Phys. Lett. B **618**, 90 (2005).
- [8] A. Bacchetta *et al.*, JHEP **0702**, 093 (2007).
- [9] A. Metz *et al.*, Prog. Part. Nucl. Phys. **91**, 136 (2016).
- [10] B. Pasquini and S. Rodini, Phys. Lett. B **788**, 414 (2019).
- [11] D. W. Sivers, Phys. Rev. D **43**, 261 (1991).
- [12] A. V. Efremov, K. Goeke, and P. Schweitzer, Phys. Rev. D **67**, 114014 (2003).
- [13] A. Bacchetta, U. D’Alesio, M. Diehl, and C. A. Miller, Phys. Rev. D **70**, 117504 (2004).
- [14] A. Metz and M. Schlegel, Eur. Phys. J. A **22**, 489 (2004).
- [15] M. Anselmino, M. Boglione, U. D’Alesio, S. Melis, F. Murgia and A. Prokudin, Phys. Rev. D **87**, 094019 (2013).
- [16] M. Anselmino *et al.*, Prog. Part. Nucl. Phys. **114**, 103806 (2020).
- [17] A. Airapetian *et al.* (*HERMES Collaboration*), Phys. Rev. Lett. **84**, 4047 (2000).
- [18] A. Airapetian *et al.* (*HERMES Collaboration*), Phys. Lett. B **648**, 164 (2007).
- [19] A. Airapetian *et al.* (*HERMES Collaboration*), Phys. Lett. B **797**, 134886 (2019).
- [20] C. Adolph *et al.* (*COMPASS Collaboration*), Nucl. Phys. B **886**, 1046 (2014).
- [21] W. Gohn *et al.* (*CLAS Collaboration*), Phys. Rev. D **89**, 072011 (2014).
- [22] J. Levelt and P. J. Mulders, Phys. Lett. B **338**, 357 (1994).
- [23] S. Bastami *et al.*, JHEP **06**, 007 (2019).
- [24] A. V. Efremov and P. Schweitzer, JHEP **08**, 006 (2003).
- [25] C. Cebulla, J. Ossmann, P. Schweitzer and D. Urbano, Acta Phys. Polon. B **39**, 609 (2008).
- [26] V.D. Burkert *et al.* (*CLAS Collaboration*), NIM A **959**, 163419 (2020).
- [27] See supplemental material (link).
- [28] CLAS physics database, <https://clas.sinp.msu.ru/cgi-bin/jlab/db.cgi>.
- [29] W. Mao and Z. Lu, Eur. Phys. J. C **73**, 2557 (2013).
- [30] W. Mao and Z. Lu, Eur. Phys. J. C **74**, 2910 (2014).
- [31] S. Bastami, K. Tezgin, A. Prokudin and P. Schweitzer, private communication (2020).
- [32] A. Bacchetta, F. Conti and M. Radici, Phys. Rev. D **78**, 074010 (2008).
- [33] S. Chekanov *et al.*, Phys. Rev. D **67**, 012007 (2003).
- [34] M. Gluck, E. Reya, M. Stratmann and W. Vogelsang, Phys. Rev. D **63**, 094005 (2001).
- [35] M. Y. Barabanov *et al.*, *Diquark Correlations in Hadron Physics: Origin, Impact and Evidence*, [arXiv:2008.07630 [hep-ph]], Prog. Part. Nucl. Phys. (2020) *in press*.
- [36] M. Anselmino, M. Boglione, U. D’Alesio, A. Kotzinian, F. Murgia, A. Prokudin and S. Melis, Nucl. Phys. Proc. Suppl. **191**, 98 (2009).
- [37] P. Schweitzer, Phys. Rev. D **67**, 114010 (2003).
- [38] Y. Ohmishi and M. Wakamatsu, Phys. Rev. D **69**, 114002 (2004).